Advances in Nano Research, *Vol. 10, No. 1 (2021) 43-57*
DOI: https://doi.org/10.12989/anr.2021.10.1.043

On thermally induced instability of FG-CNTRC cylindrical panels

Razieh Hashemi[1a], Mostafa Mirzaei[*2] and Mohammad R. Adlparvar[1b]

[1]*Department of Civil Engineering, Faculty of Engineering, University of Qom, Alghadir Blvd, Qom, Iran*
[2]*Department of Mechanical Engineering, Faculty of Engineering, University of Qom, Alghadir Blvd, Qom, Iran*

(*Received October 27, 2019, Revised September 15, 2020, Accepted September 29, 2020*)

Abstract. In this study, thermally induced bifurcation buckling of shallow composite cylindrical panels reinforced with aligned single-walled carbon nanotubes is investigated. Distribution of carbon nanotubes across the thickness of the cylindrical panel as reinforcements may be either uniform or functionally graded. Thermo-mechanical properties of the matrix and reinforcements are considered to be temperature dependent. Properties of the cylindrical panel are obtained using a refined micromechanical approach which introduces the auxiliary parameters into the rule of mixtures. The governing equations are obtained by using the static version of the Hamilton principle based on the first-order shear deformation theory and considering the linear strain-displacement relation. An energy-based Ritz method and an iterative process are used to obtain the critical buckling temperature of composite cylindrical panel with temperature dependent material properties. In addition, the effect of various parameters such as the boundary conditions, different geometrical conditions, distribution pattern of CNTs across the thickness and their volume fraction are studied on the critical buckling temperature and buckled pattern of cylindrical panels. It is shown that FG-X type of CNT dispersion is the most influential type in thermal stability.

Keywords: thermal buckling; FG-CNTRC; cylindrical panel; Ritz method; temperature dependent properties

1. Introduction

Thin structures in the form of cylindrical shells and curved panels are widely used in aerospace engineering and civil applications. These structures are frequently exposed to complex loading conditions and their stability is a significant problem attracting interest of many researchers. On the other hand, there is always an essential demand to use novel materials with improved properties in the industry. The reports of material scientists proven that Carbon Nanotubes (CNTs) possess extremely high elastic moduli and very superior electrical and thermal properties with very large aspect ration. There are two main types of CNTs: Single-Walled Carbon Nanotubes (SWCNTs) and Multi-Walled Carbon Nanotubes (MWCNTs). There is No previous material displaying extraordinary mechanical, thermal and electrical properties as CNTs (Amir *et al*. 2019, Ansari and Kumar 2019, Rezaiee-Pajand *et al*. 2019, Shahedi and Mohammadimehr 2019, Yazdi 2019). Due to wonderful properties, CNTs are used as excellent reinforcements in a polymer matrix to obtain Carbon Nanotube-Reinforced Composite (CNTRC) known as an advanced nanocomposite (Hussain *et al.* 2019, 2020, Asghar *et al*. 2020). These composites are widely used in industrial applications and have promising potential for numerous applications in the future.

For the first time, the mechanical behavior of Functionally Graded Carbon Nanotube Reinforced Composite (FG-CNTRC) structures has been analyzed by Shen (2009). In this research, the nonlinear bending of the composite plate in thermal environments has been investigated. The results of this research show the excellent properties of CNTs as reinforcements. After this study, many researchers perused the linear or nonlinear behavior of composite structures under different loading conditions. Various numerical and analytical methods have been applied to solve these problems that a summary of these recent studies is expressed here.

Employing a semi-analytical method based on the two-perturbation technique, Shen (2016) analyzed the post-buckling behavior of FG-CNTRC cylindrical panels under external pressure. In this work, the influences of geometrical properties of the panel, elastic foundation and temperature dependence of material properties have been included in the formulations.

Mirzaei and Kiani (2016a) performed an investigation on the free vibration of FG-CNTRC cylindrical panels. The natural frequency of the panel has been obtained by using the FSDT, the Hamilton principle and Chebyshev polynomials as the basic functions of the Ritz method. The reports show that natural frequency increases by increasing the volume fraction of carbon nanotubes and among the five patterns of distribution of CNTs across the panel thickness, the higher frequencies belong to the FG-X panels and FG-O panels have the minimum frequencies. Using a similar approach, the critical buckling temperature of FG-CNTRC plates under uniform heating has been investigated by Mirzaei and Kiani (2016b). Material properties of FG-CNTRC composite plates have been assumed to be

*Corresponding author, Professor,
E-mail: m.mirzaei@qom.ac.ir
[a] M.Sc.
[b] Ph.D.

ISSN: 2287-237X (Print), 2287-2388 (Online)

temperature dependent. In other research, utilizing ARC-length method and modified Newton-Raphson algorithm, Zhang and Liew (2016) and Zhang *et al*. (2016) investigated buckling and post-buckling behavior of axially compressed FG-CNTRC plates taking effects of elastic foundation and elastic restraints of edges. Kiani (2017b) employed the von-Kármán type of geometrical nonlinearly, First-order Shear Deformation plate Theory (FSDT) and Ritz method to analyze the thermal post-buckling equilibrium paths of the FG-CNTRC plates. The results of this study show that FG-CNTRC plates under uniform heating, reveal the secondary instability which is designated with a snap through motion in the post-buckling equilibrium path.

A linear buckling analysis of CNTRC cylindrical panels under axial compression and shear has been performed by Garcia *et al*. (2017) utilizing the Finite Element method (FEM). Hieu and Tung (2018) studied the buckling and post-buckling behaviors of thin CNTRC cylindrical shells surrounded by elastic media under combined loads of axial compression and lateral pressure in thermal environments. Also, Trang and Tung (2018) performed an investigation of the nonlinear stability of thin CNTRC cylindrical panels with elastically restrained straight edges under combined thermomechanical loading conditions using the Galerkin method. Also, based on an analytical approach, Tung and Trang (2018) studied buckling and post-buckling behaviors of FG-CNTRC plates with tangentially restrained edges resting on elastic foundations under thermal loading using the Galerkin method and iteration algorithms.

Employing a numerical approach based on the shear deformation theory and Variational Differential Quadrature (VDQ) method Torabi and Ansari (2018) analyzed the impacts of thermal loading on the vibration and buckling of temperature-dependent FG-CNTRC conical shells.

Ebrahimi and Farazmandnia (2018a, b) performed an investigation on vibration and thermo-mechanical buckling analysis of sandwich beams with a stiff core and face sheets made of FG-CNTRC within the framework of Timoshenko beam theory. In their study, the governing equations and boundary conditions are derived using Hamilton's principle and solved utilizing an efficient technique called the Differential Transform Method (DTM).

Mehar and Panda (2019) performed the thermal buckling analysis of the FG-CNTRC shell panel based on the Higher-order Shear Deformation Theory (HSDT) mid-plane kinematics using the finite element method and highlighted the effect of various design parameters on the thermal instability of composite shell panel reinforced with CNTs. Chan *et al*. (2019) investigated the nonlinear buckling and post-buckling of FG-CNTRC truncated conical shells under axial load using Airy stress function and the Galerkin method based on the classical shell theory.

Karami and Karami (2019) performed an investigation on the buckling analysis of size-dependent rectangular plates made of temperature-dependent Functionally Graded Materials (FGMs). In this research, Material properties have been obtained based on Reuss micromechanical model and a semi-numerical solution has been applied to find the critical buckling force of the nanoplate.

Draoui *et al*. (2019) invented a theory based on the FSDT theory for the static and dynamic behavior of carbon nanotube-reinforced composite sandwich plates using. Two types of plates are used: (1) Sandwich with reinforced face sheet and homogeneous core and (2) sandwich with homogeneous face sheet and reinforced core.

The static and dynamic behavior of FG-CNT reinforced porous sandwich polymer plate have been analyzed by Medani *et al*. (2019) utilizing the Hamilton's principle and FSDT. Two types of porous sandwich plates are supposed (sandwich with face sheets reinforced/ homogeneous core and sandwich with homogeneous face sheets/ reinforced core).

Ebrahimi *et al*. (2019) presented the thermal buckling analysis of embedded graphene-oxide powder-reinforced nanocomposite plates under three types of thermal loading. The effective material properties of the nanocomposite plate have been obtained according to the Halpin-Tsai micromechanical scheme. The governing equations have been derived based on a refined HSDT and Hamilton's principle and solved analytically via Navier's solution for a simply supported nanocomposite plate. In other research, using a Simple First-order Shear Deformation Theory (SFSDT) and Navier solution procedure based on an analytical model, Draiche *et al*. (2019) predicted the static analysis of laminated reinforced composite plates subjected to sinusoidal and uniform loads. The most important aspect of this study is that unlike the conventional FSDT, the proposed model has contained only four unknown variables. Also, by applying the integral-first shear deformation theory and Navier solution, buckling and dynamic behavior of the simply supported CNT-RC beams have been investigated by Bousahla *et al*. (2020). In all cases, the Navier solution is only used for the simply supported structures.

Based on an analytical solution and employing a simple quasi-3D shear deformation theory and Navier method, Zarga *et al*. (2019) studied thermo-mechanical bending analysis of functionally graded material sandwich plates. The displacement field is defined using only five variables as the FSDT. Unlike the other high order shear deformation theories, the formulation of this present considers a new kinematic which includes undetermined integral variables.

Using an efficient and original high-order shear and normal deformation theory and Hamilton's principle, Khiloun *et al*. (2020) examined the static and free vibration analysis of functionally graded plates. Also, Kaddari *et al*. (2020) investigated the statics and free vibration behavior of functionally graded porous plates resting on elastic foundations using a similar method.

Based on third-order shear deformation theory and using the Generalized Differential Quadrature Method (GDQM), the buckling temperature and post-buckling analysis of Functionally Graded Graphene nanoplatelet-Reinforced Composite (FG-GPLRC) disk covered with a piezoelectric actuator and surrounded by the nonlinear elastic foundation have been investigated by Al-Furjan *et al*. (2020).

Tayeb Si *et al*. (2020) obtained the critical buckling load of a FG-CNTs reinforced composite plate using Hamilton's energy principle. In this research, based on the Mindlin-Reissner theory that takes into account the transversal shear

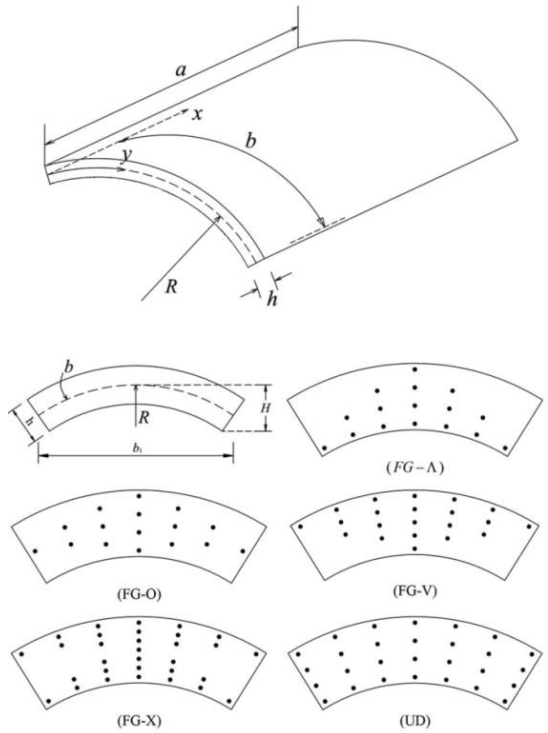

Fig. 1 Geometry and coordinate system of a cylindrical panel and different types of carbon nanotube distributions

effect, for mechanical buckling analysis of the polymer plate with parabolic distribution of carbon nanotubes. The results show that the critical buckling load of parabolic distribution is larger than the linear distribution.

The linear free vibration of FG-CNT reinforced composite cylindrical panels with cutout has been investigated by Mirzaei (2020). In this study, the natural frequencies have been obtained by Ritz method with Chebyshev polynomials. This method is used for different boundary conditions. Qin *et al*. (2020) used the unified Fourier series solution for linear vibration analysis of FG-CNTRC cylindrical, conical shells and annular plates with arbitrary boundary conditions. Hieu and Tung (2020) performed an investigation on thermal and thermo-mechanical buckling of shear deformable FG-CNTRC cylindrical shells and toroidal shell segments with tangentially restrained edges by Galerkin method. Using the finite difference differential, the buckling and vibration analyses of cracked FG cylindrical panel under external pressure have been investigated by Torabi and Ansari (2020).

As seen from the above literature review, there is no work on the thermal buckling analysis of FG-CNTRC cylindrical panel with different boundary condition and nonsymmetric distributions of CNTs using Chebyshev polynomials and Ritz solution method. The aim of this study is to obtain the critical buckling temperature of FG-CNTRC cylindrical panels under uniaxial or biaxial in-plane thermal loading via a Ritz method. To establish the governing equations of the panel at the onset of buckling, the first order shear deformation theory is used. Chebyshev polynomials are used as the basis of the shape functions for arbitrary boundary conditions such as clamped, simply supported, sliding supported and free. An eigenvalue problem is established to acquire the critical buckling temperature of temperature dependent FG-CNTRC cylindrical panel. In this research, comparison studies are done to validate the assumed method and parametric studies are given to investigate the effect of various parameters such as the volume fraction of carbon nanotubes, distribution of CNTs, geometrical properties and boundary condition. It is shown that all of the above-mentioned parameters are effective on the buckling temperature and buckled shapes of the cylindrical panel.

2. Basic formulation

The aim of this study is to obtain the critical buckling temperature of FG-CNTRC cylindrical panel. An FG-CNTR panel is considered with constant thickness *h*, curved edge *b* straight edge *a* and radius of curvature *R* that, shown in Fig. 1. The above panel is made of a polymer matrix reinforced with SWCNT. The coordinate system is assigned to the middle of the mid-surface of the panel where as usual $-0.5a \le x \le +0.5a$ is through the length, $-0.5b \le y \le +0.5b$ is through the width and $-0.5h \le z \le +0.5h$ is through the thickness. Distribution of carbon nanotubes across the thickness of the panel may be uniform (referred to as UD) or functionally graded (referred to as FG) (Zhang *et al*. 2016, Shen and Wang 2017, Zhang and Xiao 2017, Shen and He 2017).

In this study, four types of functionally graded distribution of SWCNTs and the uniform distribution are considered. FG-V, FG-O, FG-Λ and FG-X CNTRC are functionally graded distributions of SWCNTs through the thickness direction of the composite cylindrical panel. Thermo-mechanical properties of the cylindrical panel are obtained by using the well-known homogenization schemes, such as Mori-Tanaka scheme or the rule of mixtures (Kiani *et al*. 2018). In the present study, the rule of mixtures is used to obtain the properties of the composite cylindrical panel, for the sake of simplicity. According to the extended rule of mixtures (Zhang *et al*. 2016, Mirzaei 2018), the effective material properties of CNTRC panel can be expressed as

$$\begin{aligned} E_{11} &= \eta_1 V_{CNT} E_{11}^{CNT} + V_m E^m \\ \frac{\eta_2}{E_{22}} &= \frac{V_{CNT}}{E_{22}^{CNT}} + \frac{V_m}{E^m} \\ \frac{\eta_3}{G_{12}} &= \frac{V_{CNT}}{G_{12}^{CNT}} + \frac{V_m}{G^m} \end{aligned} \tag{1}$$

$E_{11}^{CNT}, E_{22}^{CNT}$ and G_{12}^{CNT} indicate Young's modulus and shear modulus of SWCNTs, E^m and G^m represent the corresponding properties of the isotropic matrix respectively. Besides, in the above equations η_j, j = 1, 2, 3 are the so-called efficiency parameters. These parameters are introduced to capture the size-dependent material properties of the FG-CNTRC panel and are determined by matching the results of a Molecular Dynamics (MD) or

Table 1 Volume fraction of CNTs as a function of thickness coordinate for various cases of CNTs distribution (Kiani 2017a)

CNTs distribution	V_{CNT}
UD	V_{CNT}^{*}
FG-Λ	$(1-\frac{2z}{h})V_{\mathrm{CNT}}^{*}$
FG-V	$(1+\frac{2z}{h})V_{\mathrm{CNT}}^{*}$
FG-O	$(1-\frac{2\lvert z\rvert}{h})V_{\mathrm{CNT}}^{*}$
FG-X	$2(\frac{2\lvert z\rvert}{h})V_{\mathrm{CNT}}^{*}$

multi-scale simulation with the results from the rule of mixtures (Kiani 2018). Also, In Eq. (1), volume fraction of SWCNTs and matrix are denoted by V_{CNT} and V_m respectively which satisfy the condition (Kiani 2017a)

$$V_{CNT}+V_m=1 \tag{2}$$

In the present research, as mentioned earlier, five types of SWCNT distributions across the thickness of the panel are considered. In Table 1 distribution function of CNTs across the panel thickness is provided. The total volume fraction across the panel thickness in all of these cases is equal to. In FG-X type, distribution of CNT is maximum near the outer and inner surfaces whereas the mid-plane is free of CNTs. However, For FG-O distribution, outer and inner surfaces are free of CNTs and the mid-surface of the panel is enriched with CNTs. In FG-V, the outer surface is enriched with CNTs and the inner surface is free of CNTs. Type FG-Λ is inverse and the inner surface has the maximum volume fraction of CNT whereas the outer surface is free of CNTs. In UD type, each surface of the panel through the thickness has the same volume fraction of CNTs (Kiani 2017a). Distribution types of carbon nanotubes in cylindrical panels are shown in Fig. 1. The effective Poisson ratio depends weakly on position (Mirzaei 2020) and is expressed as

$$\nu_{12}=V_{CNT}\nu_{12}^{CNT}+V_m\nu^m \tag{3}$$

where Poisson ratio of SWCNTs and matrix are denoted by ν_{12}^{CNT} and ν^m respectively.

Following the Shapery model, longitudinal and transverse thermal expansion coefficients are expressed as (Mirzaei and Kiani 2016b)

$$\begin{aligned}\alpha_{11}&=\frac{V_{CNT}E_{11}^{CNT}\alpha_{11}^{CNT}+V_mE^m\alpha^m}{V_{CNT}E_{11}^{CNT}+V_mE^m}\\ \alpha_{22}&=(1+\nu_{12}^{CNT})V_{CNT}\alpha_{22}^{CNT}+(1+\nu^m)V_m\alpha^m-\nu_{12}\alpha_{11}\end{aligned} \tag{4}$$

In the above equation, α_{11}^{CNT}, α_{22}^{CNT} and α^m are the thermal expansion coefficients of the constituents.

In order to consider the effects of through the thickness shear deformation, the first order shear deformation shell theory is used (Leissa 1986, Qatu and Leissa 1993, Reddy 2003, Aydogdu 2008). According to the first order shear deformation shell theory, displacement components of the shell may be written in terms of the characteristics of the mid-surface of the shell and cross section rotations as (Kiani 2016, Mirzaei 2018)

$$\begin{Bmatrix}u(x,y,z)\\ v(x,y,z)\\ w(x,y,z)\end{Bmatrix}=\begin{Bmatrix}u_0(x,y)+z\phi_x(x,y)\\ v_0(x,y)+z\phi_y(x,y)\\ w_0(x,y)\end{Bmatrix} \tag{5}$$

In the above equations, displacement components u, v and w are associated to displacements along x, y and z directions, respectively. Besides, a subscript 0 indicates the characteristics of the mid-surface. Transverse normal rotations about the x and y axes are denoted by φ_x and φ_y respectively.

According to the first order shell theory, in-plane strain components are written in terms of mid-surface strains and change in curvatures. Besides, through-the-thickness shear strain components are assumed to be constant. Therefore, one may write (Draoui *et al*. 2019 and Matouk *et al*. 2020)

$$\begin{Bmatrix}\varepsilon_{xx}\\ \varepsilon_{yy}\\ \gamma_{xy}\\ \gamma_{xz}\\ \gamma_{yz}\end{Bmatrix}=\begin{Bmatrix}\varepsilon_{xx}^0\\ \varepsilon_{yy}^0\\ \gamma_{xy}^0\\ \gamma_{xz}^0\\ \gamma_{yz}^0\end{Bmatrix}+z\begin{Bmatrix}k_{xx}\\ k_{yy}\\ k_{xy}\\ k_{xz}\\ k_{yz}\end{Bmatrix} \tag{6}$$

In this study, a cylindrical panel under the action of uniform heating is under investigation. At least on two parallel edges of the panel normal to edge displacements are restrained. Under such conditions, the cylindrical panel cannot go thermal expansion at least along one direction and compressive thermal stresses are induced. Therefore, buckling phenomenon may happen. It is known that buckling is a nonlinear phenomenon which should be obtained under geometrically nonlinear analysis. Meanwhile, when only bifurcation buckling is of interest, the stability equations are linearized. Therefore, to obtain the stability equations associated with the onset of buckling, strain components may be assumed to be infinitesimal and therefore linear strain-displacement relations suffice. In such solution method, the potential energy due to the pre-buckling forces should be included as is shown in the next. Considering the above-mentioned discussions, the components of the strain associated to the mid-surface of the panel are linearized and are equal to (Leissa 1986, Qatu and Leissa 1993, Mirzaei and Kiani 2016b)

$$\begin{Bmatrix}\varepsilon_{xx}^0\\ \varepsilon_{yy}^0\\ \gamma_{xy}^0\\ \gamma_{xz}^0\\ \gamma_{yz}^0\end{Bmatrix}=\begin{Bmatrix}u_{0,x}\\ v_{0,y}+\frac{w_0}{R}\\ u_{0,y}+v_{0,x}\\ \phi_x+w_{0,x}\\ \phi_y+w_{0,y}\end{Bmatrix} \tag{7}$$

In above-mentioned equations and in the rest of this manuscript $(\,)_{,x}$ and $(\,)_{,y}$ denote the derivatives with respect to the x and y directions, respectively.

In Eq. (6), the components of change in curvature based on the first order shear deformation theory are equal to (Mirzaei 2020)

$$\begin{Bmatrix} k_{xx} \\ k_{yy} \\ k_{xy} \\ k_{xz} \\ k_{yz} \end{Bmatrix} = \begin{Bmatrix} \phi_{x,x} \\ \phi_{y,y} \\ \phi_{x,y} + \phi_{y,x} \\ 0 \\ 0 \end{Bmatrix} \tag{8}$$

For linear thermoelastic materials, stress field may be written as a linear function of strain field and temperature change as

$$\begin{Bmatrix} \sigma_{xx} \\ \sigma_{yy} \\ \tau_{xy} \\ \tau_{xz} \\ \tau_{yz} \end{Bmatrix} = \begin{bmatrix} Q_{11} & Q_{12} & 0 & 0 & 0 \\ Q_{12} & Q_{22} & 0 & 0 & 0 \\ 0 & 0 & Q_{66} & 0 & 0 \\ 0 & 0 & 0 & Q_{55} & 0 \\ 0 & 0 & 0 & 0 & Q_{44} \end{bmatrix} \times \begin{Bmatrix} \varepsilon_{xx} - \alpha_{11}\Delta T \\ \varepsilon_{yy} - \alpha_{22}\Delta T \\ \gamma_{xy} \\ \gamma_{xz} \\ \gamma_{yz} \end{Bmatrix} \tag{9}$$

where ΔT is temperature change. Also, T_0 and T are the reference temperature and elevated temperature respectively. Furthermore, Q_{ij}'s (i, j = 1, 2, 4, 5, 6) are the reduced material stiffness coefficients with the plane-stress conditions and are obtained as (Mirzaei and Kiani 2016b)

$$\begin{aligned} Q_{11} &= \frac{E_{11}}{1-\nu_{12}\nu_{21}}, & Q_{22} &= \frac{E_{22}}{1-\nu_{12}\nu_{21}} \\ Q_{12} &= \frac{\nu_{21}E_{11}}{1-\nu_{12}\nu_{21}}, & Q_{44} &= G_{23} \\ Q_{55} &= G_{13}, & Q_{66} &= G_{12} \end{aligned} \tag{10}$$

The in-plane force resultants, moment resultants and transverse force resultant of FSDT are obtained upon the integration of stress field through the thickness. Stress resultant components in this case become

$$\begin{Bmatrix} N_{xx} \\ N_{yy} \\ N_{xy} \\ M_{xx} \\ M_{yy} \\ M_{xy} \\ Q_{xz} \\ Q_{yz} \end{Bmatrix} = \int_{-0.5h}^{+0.5h} \begin{Bmatrix} \sigma_{xx} \\ \sigma_{yy} \\ \tau_{xy} \\ z\sigma_{xx} \\ z\sigma_{yy} \\ z\tau_{xy} \\ \kappa\tau_{xz} \\ \kappa\tau_{yz} \end{Bmatrix} dz \tag{11}$$

where, the quantities (N_{xx}, N_{yy}, N_{xy}) are called, the in-plane force resultants, (M_{xx}, M_{yy}, M_{xy}) are called the moment resultants, and (Q_{xz}, Q_{yz}), denotes the transverse force resultants. Also, in Eq. (11), κ is the shear correction factor of FSDT. Selection of a shear correction factor results in more accurate buckling loads and somehow compensate the errors due to the assumption of uniform transverse strains. Evaluation of accurate shear correction is not straightforward. Accurate studies show that this factor depends on the boundary conditions, material properties and geometry and type of loading. However, for FG-CNTRC beams, cylindrical panels and shells, the value of κ is used as κ = 1/2, κ = 5/6 or $\kappa = \pi^2/12$ and $\kappa = 5/(6 - \nu_{12})$ (Reddy 2003). In this study, this factor is chosen as κ = 5/6.

Substitution of Eq. (9) into Eq. (11) with the simultaneous aid of Eqs. (5)-(8) and (10) generates the stress resultants in terms of the mid-surface characteristics of the cylindrical panel as

$$\begin{Bmatrix} N_{xx} \\ N_{yy} \\ N_{xy} \\ M_{xx} \\ M_{yy} \\ M_{xy} \\ Q_{xz} \\ Q_{yz} \end{Bmatrix} = \begin{bmatrix} A_{11} & A_{12} & 0 & B_{11} & B_{12} & 0 & 0 & 0 \\ A_{12} & A_{22} & 0 & B_{12} & B_{22} & 0 & 0 & 0 \\ 0 & 0 & A_{66} & 0 & 0 & B_{66} & 0 & 0 \\ B_{11} & B_{12} & 0 & D_{11} & D_{12} & 0 & 0 & 0 \\ B_{12} & B_{22} & 0 & D_{12} & D_{22} & 0 & 0 & 0 \\ 0 & 0 & B_{66} & 0 & 0 & D_{66} & 0 & 0 \\ 0 & 0 & 0 & 0 & 0 & 0 & \kappa A_{55} & 0 \\ 0 & 0 & 0 & 0 & 0 & 0 & 0 & \kappa A_{44} \end{bmatrix} \times \begin{Bmatrix} \varepsilon_{xx}^0 \\ \varepsilon_{yy}^0 \\ \gamma_{xy}^0 \\ k_{xx} \\ k_{yy} \\ k_{xy} \\ \gamma_{xz}^0 \\ \gamma_{yz}^0 \end{Bmatrix} - \begin{Bmatrix} N_{xx}^T \\ N_{yy}^T \\ 0 \\ M_{xx}^T \\ M_{yy}^T \\ 0 \\ 0 \\ 0 \end{Bmatrix} \tag{12}$$

In Eq. (12), the stiffness components A_{ij}, B_{ij} and D_{ij} indicate the stretching, bending-stretching and bending stiffnesses, respectively, which are calculated by (Mirzaei 2020)

$$(A_{ij}, B_{ij}, D_{ij}) = \int_{-0.5h}^{+0.5h} (Q_{ij}, zQ_{ij}, z^2Q_{ij})dz \tag{13}$$

Also, N_{ii}^T, M_{ii}^T, $i = x, y$ are the thermally induced force and moment resultants which are obtained upon calculation of stress resultants as

$$\begin{bmatrix} N_{xx}^T & M_{xx}^T \\ N_{yy}^T & M_{yy}^T \end{bmatrix} = \int_{-0.5h}^{+0.5h} \begin{bmatrix} Q_{11} & Q_{12} \\ Q_{12} & Q_{22} \end{bmatrix} \begin{bmatrix} \alpha_{11} \\ \alpha_{22} \end{bmatrix} (T - T_0)[1 \quad z]dz \tag{14}$$

It is of worth-noting that, by increasing uniform temperature for FG-X, FG-O and UD types of CNT distribution, no thermal bending moments are produced. Besides, due to the symmetric distribution of CNTs across the thickness in these three cases, the stretching-bending coupling stiffness components, i.e., B_{ij}'s are all equal to zero.

Stability equations may be obtained with the aid of the static version of the Hamilton principle. At the onset of buckling, one may write (Reddy 2003)

$$\delta(U + V) = 0 \tag{15}$$

where δU is the virtual strain energy of the thermoelastic of the cylindrical panel which may be calculated as (Mirzaei 2018)

$$\delta U = \int_{-0.5a}^{+0.5a}\int_{-0.5b}^{+0.5b}\int_{-0.5h}^{+0.5h}(\sigma_{xx}\delta\varepsilon_{xx} + \sigma_{yy}\delta\varepsilon_{yy} + \tau_{xy}\delta\gamma_{xy} + \tau_{xz}\delta\gamma_{xz} + \tau_{yz}\delta\gamma_{yz})dzdydx \quad (16)$$

and δV is the virtual potential energy of the pre-buckling loads due to the constant uniform heating. It is of worth-noting that, even under uniform heating, bifurcation phenomenon may not occur. Considering the distributed patterns of CNTs across the cylindrical panel thickness, in this study, three symmetric patterns and one nonsymmetric pattern are taken into consideration. As mentioned earlier in FG-V type of CNT dispersion and even in uniform heating, thermal moments are generated. Obviously, the induced thermal moments enforce the cylindrical panel to deflect unless the thermally induced moments are surpassed by the supports. As known, clamped and sliding supported edges are capable of applying the additional bending moment at the support when is necessary, however, simply supported and free edges are unable to reveal such feature. Therefore, thermal buckling occurs for arbitrary type of FG-CNTRC cylindrical panel with combinations of clamped and sliding supported edges. However, for cylindrical panels with at least one edge simply supported or free, distribution of CNTs across the thickness should be symmetric. Considering that the above conditions are met for the occurrence of thermal bifurcation buckling, pre-buckling forces may be obtained according to the in-plane boundary conditions. For the case when in-plane displacement components are equal to zero at the edges (all edges are restrained again thermal expansion), pre-buckling forces are equal to thermally induced loads. Therefore, the potential energy of the pre-buckling forces at the onset of buckling is equal to Kiani (2018)

$$\delta V = -\int_{-0.5a}^{+0.5a}\int_{-0.5b}^{+0.5b}(N_{xx}^{T}w_{0,x}\delta w_{0,x} + N_{yy}^{T}w_{0,y}\delta w_{0,y})dydx \quad (17)$$

However, when two parallel edges of the panel are not restrained to move in normal to edge direction, in that direction, only thermal expansion is generated and thermal forces are not induced. In this case, pre-buckling thermal forces should be obtained using the same process developed by Jones (2005). In a cylindrical panel with free boundary conditions along $y = \pm b/2$, while the two other edges are restrained against thermal expansion, the pre-buckling forces are obtained by Jones (2005). The work done by such thermally induced forces at the onset of buckling may be written as (Mirzaei and Kiani 2016b)

$$\delta V = -\int_{-0.5a}^{+0.5a}\int_{-0.5b}^{+0.5b}\left(\frac{A_{12}}{A_{22}}N_{yy}^{T} - N_{xx}^{T}\right)\left(\frac{\partial w_0}{\partial x}\right)^2 dydx \quad (18)$$

3. Solution procedure

While the stability equations and the associated boundary conditions may be obtained by the application of Green theorem to the Eq. (15), energy-based methods also may be employed to solve the stability Eq. (15). In the present research, Ritz method with Chebyshev basis polynomials is used to derive the stability equations in a matrix representation. According to the Ritz method each of the displacement components are written in terms of a set of shape functions. Various set of functions may be used for the shape functions. Polynomial shape functions, Chebyshev polynomials or orthogonal sets obtained according to the Gram-Schmidt algorithm is used extensively. For each of the displacement components, u_0, v_0, w_0, φ_x and φ_y one may write

$$\begin{aligned}
u_0(x,y) &= R^u(x,y)\sum_{i=1}^{N_x}\sum_{j=1}^{N_y}U_{ij}P_i(x)P_j(y)\\
v_0(x,y) &= R^v(x,y)\sum_{i=1}^{N_x}\sum_{j=1}^{N_y}V_{ij}P_i(x)P_j(y)\\
w_0(x,y) &= R^w(x,y)\sum_{i=1}^{N_x}\sum_{j=1}^{N_y}W_{ij}P_i(x)P_j(y)\\
\phi_x(x,y) &= R^x(x,y)\sum_{i=1}^{N_x}\sum_{j=1}^{N_y}X_{ij}P_i(x)P_j(y)\\
\phi_y(x,y) &= R^y(x,y)\sum_{i=1}^{N_x}\sum_{j=1}^{N_y}Y_{ij}P_i(x)P_j(y)
\end{aligned} \quad (19)$$

where in the above-mentioned equation $P_i(x)$ and $P_j(y)$ are the i-th and j-th Chebyshev polynomials of the first kind which are defined by

$$\begin{aligned}
P_i(x) &= cos((i-1)arc\,cos(2x/a))\\
P_j(y) &= cos((j-1)arc\,cos(2y/b))
\end{aligned} \quad (20)$$

Besides, in Eq. (19), functions $R^{\alpha}(x,y)$, $\alpha = u, v, w, x, y$ are the boundary functions corresponding to the essential boundary conditions. It is known that in Ritz family methods, adoption of a shape function depends only on the essential boundary condition. In this research, four types of boundary conditions are used, clamped (C), simply supported (S), sliding supported (X) and free (F). For a clamped edge all of the in-plane and out-of-plane essential variables are restrained. For a simply supported edge normal and tangential displacements, lateral displacement and tangent slope are restrained and for a sliding supported edge only normal slope is restrained. At a free edge none of the boundary conditions are essential. Therefore, the essential variables associated to each of these cases may be written as

For a clamped edge

$$\begin{aligned}
x &= \pm\frac{a}{2}: \quad u_0 = v_0 = w_0 = \phi_x = \phi_y = 0\\
y &= \pm\frac{b}{2}: \quad u_0 = v_0 = w_0 = \phi_x = \phi_y = 0
\end{aligned} \quad (21)$$

For a simply supported edge

$$x = \pm\frac{a}{2}: \quad u_0 = v_0 = w_0 = \phi_y = 0 \quad (22)$$

$$y = \pm\frac{b}{2}: \quad u_0 = v_0 = w_0 = \phi_x = 0$$

For a sliding supported edge

$$\begin{aligned} x &= \pm\frac{a}{2}: \quad u_0 = v_0 = \phi_x = 0 \\ y &= \pm\frac{b}{2}: \quad u_0 = v_0 = \phi_y = 0 \end{aligned} \tag{23}$$

For a free edge

$$\begin{aligned} x &= \pm\frac{a}{2}: \quad - \\ y &= \pm\frac{b}{2}: \quad - \end{aligned} \tag{24}$$

The adoption of mechanical auxiliary functions $R^{\alpha}(x, y)$, $\alpha = u, v, w, x, y$ should be chosen according to essential boundary conditions on each side. Each of the functions R^{α} may be written as

$$R^{\alpha}(x,y) = \left(1+\frac{2x}{a}\right)^{p}\left(1-\frac{2x}{a}\right)^{q}\left(1+\frac{2y}{b}\right)^{r}\left(1-\frac{2y}{b}\right)^{s} \tag{25}$$

where each of the variables p, q, r and s depends on the essential boundary conditions and are equal to zero or one. For instance, for a panel which is clamped at $x = -0.5a$ and $x = +0.5a$, free at $y = -0.5b$ and simply supported at $y = +0.5b$, auxiliary functions are

$$\begin{aligned} R^{u}(x,y) &= \left(1+\frac{2x}{a}\right)\left(1-\frac{2x}{a}\right)\left(1-\frac{2y}{b}\right) \\ R^{v}(x,y) &= \left(1+\frac{2x}{a}\right)\left(1-\frac{2x}{a}\right)\left(1-\frac{2y}{b}\right) \\ R^{w}(x,y) &= \left(1+\frac{2x}{a}\right)\left(1-\frac{2x}{a}\right) \\ R^{x}(x,y) &= \left(1+\frac{2x}{a}\right)\left(1-\frac{2x}{a}\right) \\ R^{y}(x,y) &= \left(1+\frac{2x}{a}\right)\left(1-\frac{2x}{a}\right)\left(1-\frac{2y}{b}\right) \end{aligned} \tag{26}$$

Finally, substitution of Eq. (19) into the Eq. (15) results in an eigenvalue problem as

$$(K^{e} - K^{g})X = 0 \tag{27}$$

where K_e and K_g are the elastic stiffness matrix and geometric stiffness matrix, respectively. The elastic stiffness matrix is originated from Eq. (16). Also, according to existing boundary conditions, geometric stiffness matrix is obtained from Eq. (17) or (18). Each of these matrices has $5 \times N_x \times N_y$ rows and columns. The above system should be treated as a standard eigenvalue problem to achieve the critical buckling temperature. It should be mentioned, since the properties of the constituents are temperature dependent, a successive procedure must be used to obtain the critical buckling temperature. The first step to obtain the critical buckling temperature is an evaluation of the thermo-mechanical properties of the SWCNTs and matrix at a reference temperature. Thermomechanical properties of the panel are then achieved at the obtained temperature and the eigenvalue problem is repeated again to extract a new critical buckling temperature. This procedure continues until a converged critical buckling temperature is achieved.

Table 2 Thermo-mechanical properties of (10,10) armchair SWCNT at specific temperatures (Shen and Xiang 2013) (tube length = 9.26 nm, tube means radius = 0.68 nm, tube thickness = 0.067 nm)

T (K)	E_{11}^{CNT} (TPa)	E_{22}^{CNT} (TPa)	G_{12}^{CNT} (TPa)	ν_{12}^{CNT}	$\alpha_{11}^{\mathrm{CNT}}$ (10^{-6}/K)	$\alpha_{22}^{\mathrm{CNT}}$ (10^{-6}/K)
300	5.6466	7.0800	1.9445	0.175	3.4584	5.1682
400	5.5679	6.9814	1.9703	0.175	4.1496	5.0905
500	5.5308	6.9348	1.9643	0.175	4.5361	5.0189
700	5.4744	6.8641	1.9644	0.175	4.6677	4.8943

Table 3 Efficiency parameters for different volumes of carbon nanotubes

V_{CNT}^{*}	η_1	η_2	η_3
0.12	0.137	1.022	0.7154
0.17	0.142	1.626	1.1382
0.28	0.141	1.585	1.1095

4. Numerical results and discussion

Present research aims to analyze the thermal buckling behavior of FG-CNTRC cylindrical panels with temperature dependent material properties. In this section, at first, convergence and comparison studies are conducted. Afterwards, parametric studies are performed to examine the influences of involved parameters.

In the rest of this manuscript, the following convention is established for boundary conditions. For instance, in the SCSX cylindrical panel, the first letter is associated to $x = -0.5a$, the second letter is the boundary condition at $y = -0.5b$, the third letter denotes the boundary conditions at $x = +0.5a$ and finally, the last letter is associated with the boundary at $y = +0.5b$. Unless otherwise stated, Poly (methyl methacrylate), referred to as PMMA, is selected for the matrix. Matrix material properties may be written as

$$\begin{aligned} &E^{m} = (3.54 - 0.0034T)(GPa) \\ &\nu^{m} = 0.34, \qquad \alpha^{m} = 45(1 + 0.0005\Delta T)(10^{-6}/K) \end{aligned} \tag{28}$$

In Eq. (28), $T = T_0 + \Delta T$ where $T_0 = 300$K is the reference temperature and T is measured in Kelvin. (10,10) armchair SWCNT is chosen as the reinforcement. Elasticity modulus, shear modulus, Poisson's ratio and thermal expansion coefficient of SWCNT are highly dependent on temperature. Shen and Xiang (2013) reported these properties at four certain temperature levels, i.e., T = 300, 400, 500 and 700K. The magnitudes of E_{11}, E_{22}, G_{12}, α_{11}, α_{22} and ν_{12} for CNTs at these four specific temperatures are given in Table 2.

Since this research aims to analyze the critical buckling

Table 4 Convergence study for critical buckling temperature parameter ΔT_{cr} (K) of isotropic homogeneous CCCC cylindrical Panels with various side to thickness ratios (a/b = 1, R/a = 10)

(N_x, N_y)	a/h = 10	a/h = 20	a/h = 40
(4,4)	394.5409	112.2035	31.1875
(6,6)	387.3626	109.1590	30.0701
(8,8)	387.2551	109.1198	30.0566
(9,9)	387.2423	109.1134	30.0557
(10,10)	387.2420	109.1133	30.0557
(11,11)	387.2408	109.1115	30.0554
(12,12)	387.2407	109.1114	30.0552
(13,13)	387.2407	109.1110	30.0551
(14,14)	387.2406	109.1110	30.0551
(15,15)	387.2406	109.1109	30.0551
Alkhaleefi	388.64	111.43	32.28

Table 5 Critical buckling temperatures T_{cr} (K) of SSSS FG-CNTRC rectangular cylindrical with $R = \infty$, V^*_{CNT} = 0.17 and temperature dependent material properties

Type	a/b	b/h	Shen and Zhang (2010)	Mirzaei and Kiani (2016b)	Present
UD	1.0	10	399.44	399.03	399.0236
		20	343.00	343.00	342.9927
	1.5	10	374.59	374.66	374.6574
		20	325.16	325.68	325.0867
	2.0	10	363.67	363.86	363.8521
		20	319.01	319.03	319.0273
FG-X	1.0	10	419.09	419.13	419.1193
		20	359.52	359.43	359.4193
	1.5	10	394.66	394.42	394.4082
		20	335.54	335.14	335.1283
	2.0	10	377.46	380.94	380.8368
		20	325.16	325.68	325.6853

temperature of FG-CNTRC cylindrical panels under temperature dependent assumptions, it is necessary to obtain the thermomechanical properties of the SWCNTs as a continuous function of temperature. For this purpose, each of the properties of carbon nanotubes may be written as

$$\begin{aligned} E_{11}^{CNT}(T) &= 6.3998 - 4.338417\times10^{-3}T \\ &\quad + 7.43\times10^{-6}T^2 - 4.45833\times10^{-9}T^3 \\ E_{22}^{CNT}(T) &= 8.02155 - 5.420375\times10^{-3}T \\ &\quad + 9.275\times10^{-6}T^2 - 5.5625\times10^{-9}T^3 \\ G_{12}^{CNT}(T) &= 1.40755 - 3.4765208\times10^{-3}T - \\ &\quad 6.965\times10^{-6}T^2 - 4.4791673\times10^{-9}T^3 \\ \alpha_{11}^{CNT}(T) &= -1.12515 + 0.02291688T \\ &\quad -2.887\times10^{-5}T^2 + 1.13625\times10^{-8}T^3 \\ \alpha_{22}^{CNT}(T) &= 5.43715 + 0.984625\times10^{-4}T \\ &\quad -2.9\times10^{-7}T^2 + 1.25\times10^{-11}T^3 \\ \nu_{12}^{CNT} &= 0.175 \end{aligned} \quad (29)$$

Table 6 Critical buckling temperatures T_{cr} (K) for SSSS FG-CNTRC cylindrical panels with b/R = 1, FG-X type of CNT dispersion, various aspects and side to thickness ratios

a/b	b/h	V^*_{CNT} = 0.12	V^*_{CNT} = 0.17	V^*_{CNT} = 0.28
0.8	100	335.4624	337.6515	344.7966
	50	405.5990	409.9382	427.4682
	30	527.7769	540.2639	562.5583
	20	654.6365	676.4774	664.5210
1	100	327.6749	329.3819	334.5576
	50	381.2242	385.9590	401.4977
	30	482.2093	490.1854	507.0657
	20	592.1280	608.8905	618.2366
1.2	100	323.0613	324.7331	329.4013
	50	369.9878	375.0179	389.5028
	30	444.5359	451.8005	470.3139
	20	544.6682	558.8422	579.8292
1.5	100	319.5735	321.1795	325.5690
	50	360.1473	364.1312	373.1679
	30	413.5849	420.7119	438.9757
	20	501.6759	514.8706	542.2587
2	100	317.1040	318.6232	322.9367
	50	345.6019	349.0829	357.5902
	30	391.3060	398.3755	416.2768
	20	470.6281	483.8762	514.5032
π	100	314.6610	315.7867	318.8845
	50	333.8736	336.7798	344.9417
	30	376.8457	383.6448	402.3617
	20	453.1268	466.4859	501.4054

Han and Elliott (2007) performed a molecular dynamics simulation to obtain the mechanical properties of nanocomposites reinforced with SWCNT. However in their analysis, the effective thickness of CNT is assumed to be at least 0.34 nm. The thickness of CNT as reported should be at least 0.142 nm. Therefore, Han and Elliot's research (2007) is re-examined. The so-called efficiency parameters, as stated earlier, are chosen to match the data obtained by the modified rule of mixture of the present study and the molecular dynamics simulation results. For three different volume fractions of CNTs, these parameters are as: η_1 = 0.137 and η_2 = 1.022 for V^*_{CNT} = 0.12. η_1 = 0.142 and η_2 = 1.626 for V^*_{CNT} = 0.17. η_1 = 0.141 and η_2 = 1.585 for V^*_{CNT} = 0.28.

For each case, the efficiency parameter η_3 is equal to 0.7 η_2 (Mirzaei and Kiani 2016b). In Table 3, For three different volume fractions of CNTs these parameters are obtained. The shear modulus G_{13} is taken equal to G_{12} whereas G_{23} is taken equal to $1.2G_{12}$ (Shen 2009).

4.1 Convergence and comparison studies

In this section, convergence and comparison studies are

Table 7 Thermal buckling temperatures T_{cr} (K) for FG-CNTRC cylindrical panels with a/b = 1, a/R = 1, b/h = 100, various volume fractions of CNTs, different graded pattern and combinations of S and C edges

Boundary conditions	Type	V^*_{CNT} = 0.12	V^*_{CNT} = 0.17	V^*_{CNT} = 0.28
SSSS	UD	324.7774	325.9732	328.0743
	FG-X	327.6749	329.3819	334.5576
	FG-O	322.0231	323.0408	323.7170
CCCC	UD	341.1414	341.8993	348.8757
	FG-X	349.3044	350.9380	363.8703
	FG-O	332.2945	332.8972	335.7427
CCCS	UD	339.0721	339.8274	346.6189
	FG-X	346.4773	348.1423	360.8640
	FG-O	330.6981	331.2297	334.1892
CCSS	UD	330.9907	332.0227	335.9747
	FG-X	335.9773	337.6367	345.8724
	FG-O	325.9357	326.7822	328.1988
CCSC	UD	332.7440	333.9201	337.8713
	FG-X	337.8491	339.7404	348.3233
	FG-O	327.6790	328.5869	329.8225
SCSC	UD	327.6335	329.0467	331.3459
	FG-X	330.6400	332.8463	339.0230
	FG-O	324.8542	325.8904	326.3259
SCSS	UD	325.5914	326.8548	329.0679
	FG-X	328.4769	330.3859	336.0227
	FG-O	322.8852	323.8716	324.4475
CSCS	UD	337.8500	338.6448	345.2593
	FG-X	345.0179	346.5806	359.1340
	FG-O	330.4618	330.9764	333.5009
CSSS	UD	330.9002	331.8401	335.7870
	FG-X	335.5830	337.6279	345.4891
	FG-O	325.4627	326.3407	327.9314

Table 8 Thermal buckling temperature T_{cr} (K) for FG-CNTRC cylindrical panels with a/b = 1, a/R = 1, a/h = 100, various volume fractions of CNTs, different graded pattern and combinations of C, X edges

Boundary conditions	Type	V^*_{CNT}=0.12	V^*_{CNT}=0.17	V^*_{CNT}=0.28
CCXC	UD	336.6750	337.9000	343.6307
	FG-X	340.8597	343.2858	353.8833
	FG-V	334.9842	336.3994	342.0058
	FG-Λ	333.4035	334.7134	340.2047
	FG-O	331.0397	331.7293	334.5222
CCXX	UD	331.7587	332.8036	337.9569
	FG-X	335.2965	337.4366	346.8520
	FG-V	330.5566	331.7464	337.1004
	FG-Λ	329.0501	330.0970	335.1114
	FG-O	326.8203	327.3167	330.0281
CXXX	UD	331.0805	331.8226	337.3551
	FG-X	335.2760	336.8390	345.8754
	FG-V	329.2291	330.1297	335.4452
	FG-Λ	327.4359	328.2201	333.2696
	FG-O	325.2237	325.6247	328.7233
XCXC	UD	334.3153	335.6273	341.0543
	FG-X	337.4309	339.9161	350.1499
	FG-V	333.4748	335.0093	340.7187
	FG-Λ	331.9948	333.3589	338.7338
	FG-O	330.0790	330.8046	333.5852
XCXX	UD	329.3635	330.4717	335.2626
	FG-X	331.9829	334.1378	343.0566
	FG-V	328.8332	330.1313	335. 4677
	FG-Λ	327.4555	328.5079	333.2937
	FG-O	325.6920	326.2390	328.8770

provided. At first a convergence study is given to obtain the required number of shape functions in the series expansion of the Ritz method. Convergence study is provided in Table 4. For this purpose, the critical buckling temperature of the isotropic homogeneous cylindrical panel with all edges clamped is evaluated for various numbers of the assumed shape functions. The results are compared with those obtained by Al-Khaleefi (2004) based on the finite element method with ANSYS software. The considered material properties are: E = 40 (GPa), ν = 0.25 and α = 79 × 10^{-6} (1/K). After adoption of 14 shape functions in both x and y directions highly accurate numerical results are achieved. Consequently, in the rest of this work, the number of shape functions in Ritz approximation is set equal to $N_x = N_y = 15$.

A comparison is presented in Table 5 on the critical buckling temperature parameter of FG-CNTRC cylindrical panels with flat plates. The results of this study are compared with those of Shen and Zhang (2010) and Mirzaei and Kiani (2016b). When the radius is limited to infinity, the results of critical buckling temperature of cylindrical panels are equal to the results of flat plates.

In the study of Shen and Zhang (2010), the exact solution has been presented to obtain the critical buckling temperature of FG-CNTRC plates with all edges simply supported and symmetric pattern of CNT dispersion across the plate thickness, whereas in the analysis of Mirzaei and Kiani (2016b), the Ritz solution has been implemented. Similar to Shen and Zhang (2010) the classical rule of mixtures is used to obtain the longitudinal thermal expansion coefficient of the CNTRC. Therefore only in this example and for the sake of comparison, longitudinal thermal expansion coefficient is evaluated as

$$\alpha_{11} = V_{CNT}\alpha_{11}^{CNT} + V_m\alpha^m \tag{30}$$

Critical buckling temperature of FG-CNTRC plates with two different side to thickness ratios and three different

Table 9 Critical buckling temperatures T_{cr} for SSSS FGCNTRC cylindrical panels with two parallel edges free various types of CNT dispersion, a/R = 1, a/h = 50 and V^*_{CNT} = 0.12, various aspect ratios

a/b	Type	CFCF	SFSF	SFCF	CFXF
0.8	UD	597.9868	427.5920	499.7954	519.5039
	FG-X	656.0752	466.1784	553.5720	552.5987
	FG-O	501.1000	382.9482	429.0400	480.4268
1	UD	533.0327	396.7794	451.1839	513.0425
	FG-X	592.411	424.0125	495.3005	539.4302
	FG-O	451.0670	365.5668	397.9145	449.7499
1.2	UD	485.6190	378.2470	419.7872	484.4430
	FG-X	538.5809	399.3974	455.1432	531.7946
	FG-O	419.1057	355.2762	378.9311	418.3320
1.5	UD	438.6817	361.8087	390.7523	438.1300
	FG-X	480.3734	376.4799	416.5572	497.7703
	FG-O	389.7075	346.2756	362.0493	389.1702
2	UD	395.1829	347.6185	365.1002	394.8548
	FG-X	423.2991	356.5706	381.5378	422.9895
	FG-O	363.7710	338.3874	347.4700	363.4260
π	UD	354.5563	334.2681	341.6714	354.4293
	FG-X	368.3122	338.3331	349.3225	368.1909
	FG-O	339.9366	330.1533	333.7483	339.8127

length to side ratios have been evaluated and compared with those of Shen and Zhang (2010) and Mirzaei and Kiani (2016b). The comparison is carried out in Table 5. It is seen that the results of our study match well with those of Shen and Zhang (2010) and Mirzaei and Kiani (2016b).

4.2 Parametric studies

After validating the numerical results of this study with the available data in the open literature, parametric studies are conducted in this section. Numerical results are provided in Tables 6-9 and Figs. 2-6. In all of this section, critical buckling temperature is obtained under the assumption of temperature dependent material properties.

Table 6 and Fig. 2 present the critical buckling temperature of SSSS FG-CNTRC cylindrical panels with b/R = 1, various aspect ratios, side to thickness ratios and FG-X type of CNT dispersion. Three different magnitudes are considered for the volume fraction of SWCNTs. The numerical results of this table reveal that, increasing the volume fraction of SWCNTs enhances the buckling temperature of the panel. Besides, increasing the length of the panel results in lower critical buckling temperature. Also, increasing the thickness of the panel enhances the critical buckling temperature of the panel.

Table 7 presents the critical buckling temperature of FG-CNTRC cylindrical panels. In this table, various combinations of clamped and simply supported conditions are considered for the edges. Cylindrical panels with

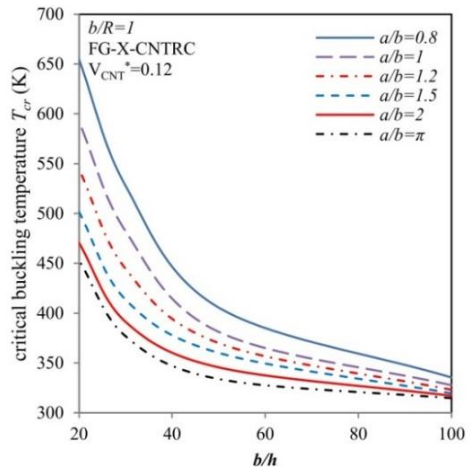

(a) Volume fraction of CNT V^*_{CNT} = 0.12

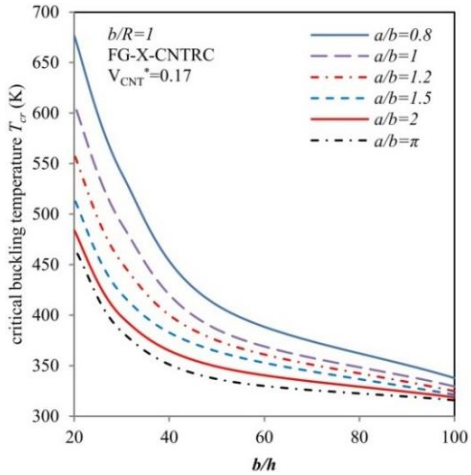

(b) Volume fraction of CNT V^*_{CNT} = 0.17

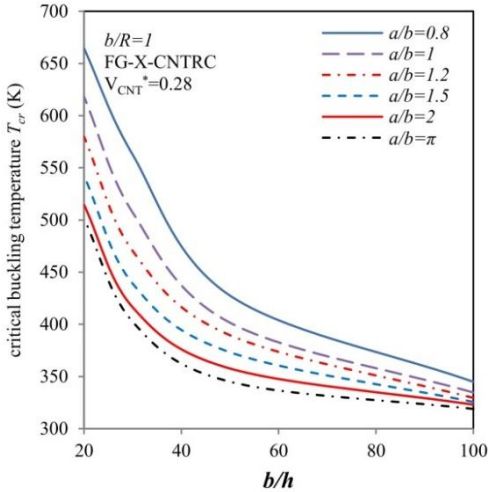

(a) Volume fraction of CNT V^*_{CNT} = 0.28

Fig. 2 Effect of length to side ratios a/b, side to thickness ratio b/h and the volume fraction of CNT on critical buckling temperature for SSSS FG-CNTRC cylindrical panels with a/R = 1 and FG-X type of SWCNT dispersion

geometrical characteristics a/b = 1, a/R = 1, a/h = 100 are considered. As already mentioned, thermal bifurcation buckling in panels with at least one edge simply supported

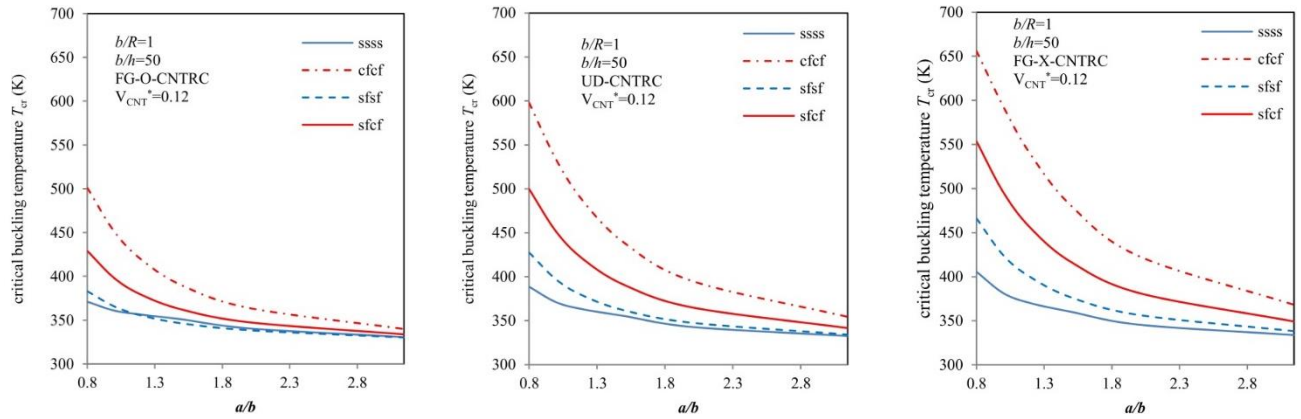

(a) FG-O distribution of carbon nanotubes (b) Uniform distribution of carbon nanotubes (c) FG-X distribution of carbon nanotubes

Fig. 3 Effect of graded pattern of SWCNTs, length to side ratios a/b and various boundary conditions on critical buckling temperature for FG-CNTRC cylindrical panels with a/R = 1, b/h = 50 and volume fraction V_{CNT}^{*} = 0.28

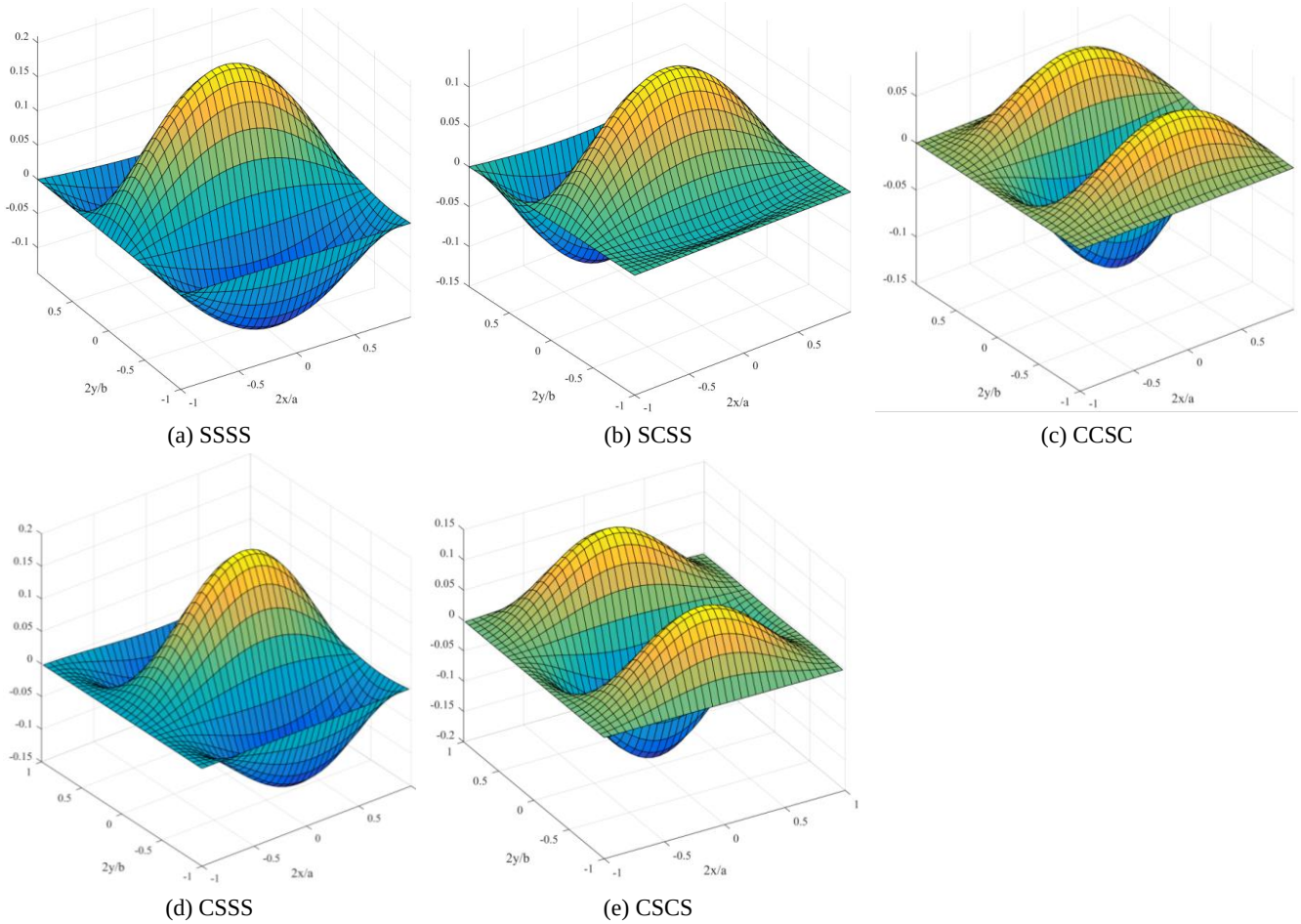

(a) SSSS (b) SCSS (c) CCSC

(d) CSSS (e) CSCS

Fig. 4 Lateral displacement mode shape of FG-CNTRC cylindrical panels with a/b = 1, b/h = 50, b/R = 1, FG-X type of CNT dispersion, volume fraction V_{CNT}^{*} = 0.28 and combinations of C and S edges

takes place when the distribution of CNTs across the thickness is symmetric with respect to the mid-plane. Therefore, only FG-X, FG-O and UD CNTRC panels are considered. Three different patterns of the CNT dispersion and three different magnitudes of volume fraction of CNTs are considered. It is seen that, in all of the studied cases, FG-X panels have higher buckling temperature than UD case and the latter dispersion profile results in higher buckling temperature in comparison to panels with FG-O type of CNT dispersion. Also, maximum buckling temperature belongs to a panel with all edges clamped and the minimum one belongs to the one with all edges simply supported. Considering various combinations of clamped and simply supported boundary conditions in panels,

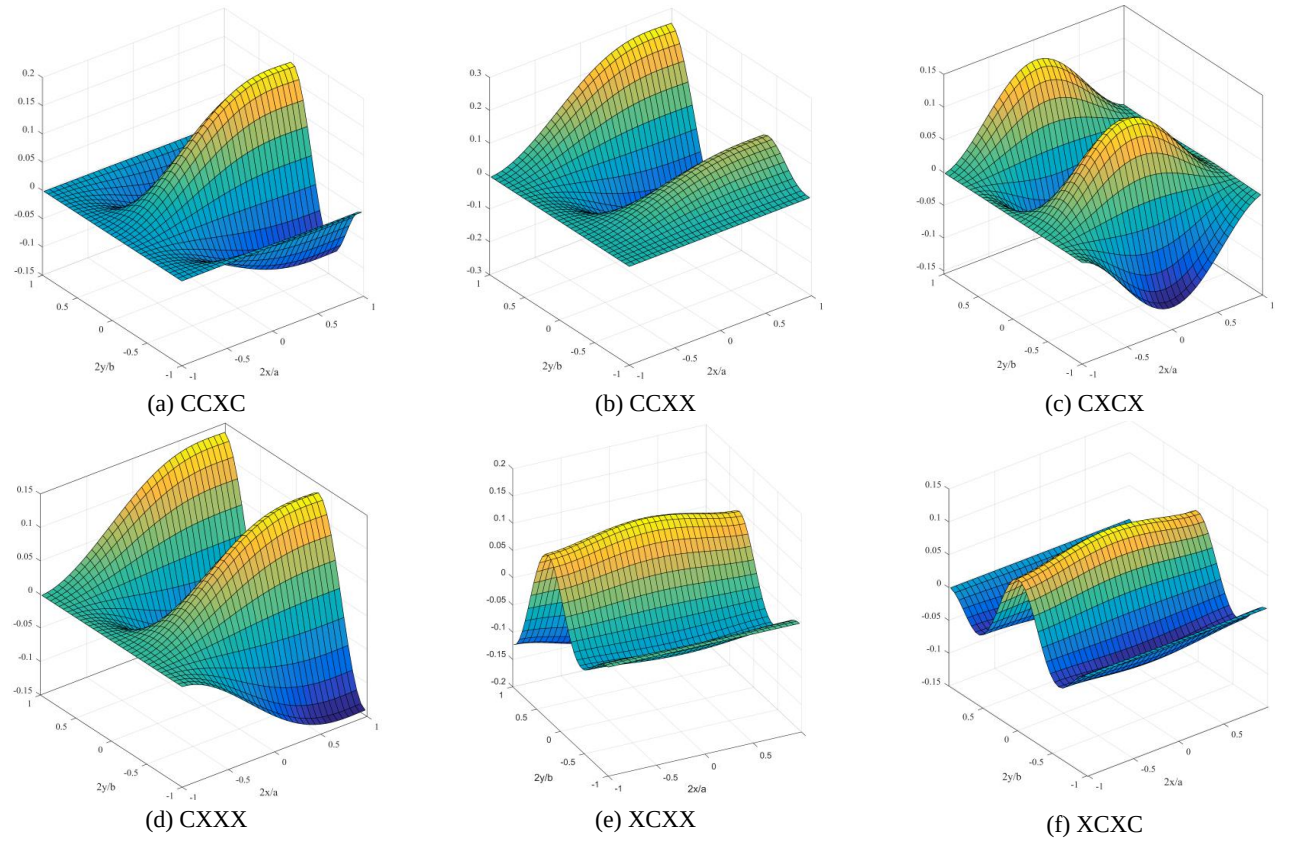

(a) CCXC (b) CCXX (c) CXCX

(d) CXXX (e) XCXX (f) XCXC

Fig. 5 Lateral displacement mode shape of FG-CNTRC cylindrical panels with a/b = 1, b/h = 50, b/R = 1, FG-X type of CNT dispersion, volume fraction V_{CNT}^{*} = 0.28 and combinations of C and X edges

numerical results reveal that critical buckling temperatures may be sorted from low to high in panels with the following boundary conditions: SSSS, SCSS, SCSC, CSSS, CCSS, CCSC, CSCS, CCCS, CCCC. It is expected that the critical buckling temperature of the clamping edge will be higher than the simply supported edge for more flexural rigidity. Considering the fact that FG-CNTRC panels are orthotropic, as seen, buckling temperature of CCCS and CCSC panels are not equal. Besides, increasing the volume fraction of carbon nanotubes enhances the critical buckling temperature of the panel. However, the effect of volume fractions of SWCNTs on the critical buckling temperature is not comparable to the effect of CNT dispersion patterns.

Table 8 presents the critical buckling temperature of FG-CNTRC panels with combinations of clamped and sliding supported edge. Both clamped and sliding support boundary conditions, are capable of applying the additional bending moment in the pre-buckling state even when the distribution of material properties is not symmetric with respect to the mid-plane.

In this table, five cases of CNT dispersion and three types of volume fraction of CNTs are considered. Geometrical characteristics of the panel are a/b = 1, b/h = 100, a/R = 1. From the numerical results of this table it is concluded that, in all of the studied cases, critical buckling temperature of the FG-Λ panel is also lower than those with FG-X type of CNT dispersion. Also, the results of this table and Table 7 indicate that, FG-X type of CNT dispersion is the most influential type in thermal stability, as also reported previously (Kiani 2016, 2017a, 2018, Mirzaei 2018). The key issue in higher critical buckling temperature of FG-X panels in comparison to the four other cases is the fact that, bending stiffnesses of the panel are much more in FG-X case since in the latter case the surfaces that are far from the mid-plane are much more enriched with SWCNTs.

Table 9 and Fig. 3 are devoted to the case of panels where two parallel edges are free and the two others are restrained against thermal expansion. As mentioned earlier in Eq. (18), a uniaxial type of buckling exists since the edges $y = \pm b/2$ are free to expand. As is obtained from Eq. (18), the compressive thermally induced force along the x direction is much lower than the one observed in biaxial thermal buckling. As a result, it is expected that critical buckling temperatures for such panels are higher than those subjected to biaxial thermal loading. For this cause, a thin panel with b/h = 50, b/R = 1 is considered and five different aspect ratios are examined. As expected, by increasing the panel length, critical buckling temperature decreases and four different types of boundary conditions are considered. Fig. 3 presents the critical buckling temperature of FG-CNTRC cylindrical panels with various aspect ratios, distribution patterns of reinforcements and boundary conditions. Volume fraction of CNT is set equal to V_{CNT}^{*} = 0.12.

Geometric characteristics of the panel are b/h = 50 and b/R = 1. The results show that critical buckling temperatures of thermally loaded SFSF panels are even higher than SSSS panels subjected to biaxial thermal compression.

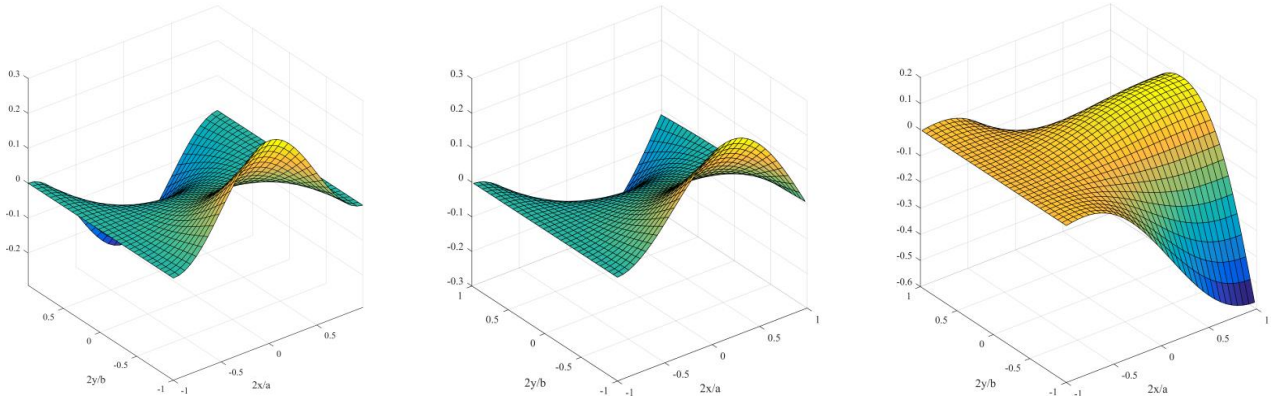

(a) CFCF (b) SFCF (c) CFXF

Fig. 6 Lateral displacement mode shape of FG-CNTRC cylindrical panels with two parallel edges free, a/b = 1, b/h = 50, b/R = 1, FG-X type of CNT dispersion, volume fraction V_{CNT}^{*} = 0.28

An example of thermal buckled shapes of FG-CNTRC cylindrical panels with a/b = 1, b/h = 50, a/R = 1 is presented in Fig. 4. Cylindrical panels with various boundary conditions comprising of S and C type of edges, FG-X type of CNT dispersion and volume fraction V_{CNT}^{*} = 0.28 are considered.

Thermal buckled shapes of FG-CNTRC square panels with various boundary conditions comprising of C and X type of edges are presented in Fig. 5. Cylindrical panels with b/h = 50, a/R = 1, FG-X type of CNT dispersion and volume fraction V_{CNT}^{*} = 0.28 are considered. It is seen that essential boundary conditions are satisfied at the supports since at the sliding supported edge lateral displacement is not restrained.

Fig. 6 demonstrates the thermally buckled pattern of FG-CNTRC cylindrical panels where two parallel edges are free and the two others are restrained against thermal expansion. Square panels with b/h = 50, a/R = 1, FG-X pattern of CNTs and volume fraction V_{CNT}^{*} = 0.28 are considered. In this Figure uniaxially loaded panels are depicted. It is observed that, essential conditions are satisfied at the edges.

5. Conclusions

In this research, thermal buckling response of functionally graded carbon nanotubes reinforced composite cylindrical panel is investigated. A composite cylindrical panel made from a polymeric matrix reinforced with SWCNTs. Properties of the SWCNTs and the polymeric matrix are assumed to be temperature dependent. Distribution of SWCNTs across thickness may be uniform or functionally graded. To obtain the thermomechanical properties of the composite panel, a refined rule of mixtures approach is developed to capture the size dependent features of SWCNTs.

The Ritz method with Chebyshev basis shape functions suitable for arbitrary boundary conditions is used to construct the eigenvalue problem associated with the critical buckling temperature and buckled shapes of the panel. Numerical examples cover the influences of volume fraction of CNTs, dispersion pattern of CNTs, boundary conditions, cylindrical panel aspect ratio and width to thickness ratio. It is shown that

• The critical buckling temperature of the FG-CNTRC cylindrical panel increases with higher CNT volume fraction (V_{CNT}^{*}).

• The critical buckling temperature of the FG-CNTRC cylindrical panel decreases with higher aspect ratio (a/b).

• The critical buckling temperature of the FG-CNTRC cylindrical panel decreases with higher width to thickness ratio (b/h).

• The critical buckling temperature for the FG-X distribution of CNTs is maximum and minimum for FG-O.

• In-plane and out-of-plane boundary conditions are influential on critical buckling temperature as well as buckled pattern of the cylindrical panel.

References

Al-Khaleefi, A.M. (2004), "Thermal buckling of clamped cylindrical panels based on first-order shear deformation theory", *Int. J. Struct. Stab. Dyn.*, **4**(3), 313-336. https://doi.org/10.1142/S0219455404001252.

Al-Furjan, M.S.H., Safarpour, H., Habibi, M., Safarpour, M. and Tounsi, A. (2020), "A comprehensive computational approach for nonlinear thermal instability of the electrically FG-GPLRC disk based on GDQ method", *Eng. Comput.*, **2020**, 1-12. https://doi.org/10.1007/s00366-020-01088-7.

Amir, S., BabaAkbar-Zarei, H. and Khorasani, M. (2019), "Flexoelectric vibration analysis of nanocomposite sandwich plates", *Mech. Based Des. Struct. Mach.*, **123**(6), 1423-1431. https://doi.org/10.1080/15397734.2019.1624175.

Ansari, M.I. and Kumar, A. (2019), "Bending analysis of functionally graded CNT reinforced doubly curved singly ruled truncated rhombic cone", *Mech. Based Des. Struct. Mach.*, **47**(1), 67-86. https://doi.org/10.1080/15397734.2018.1519635.

Asghar, S., Naeem, M.N., Hussain, M., Taj, M. and Tounsi, A. (2020), "Prediction and assessment of nonlocal natural frequencies of DWCNTs: Vibration analysis", *Comput. Concrete, Int. J.*, **25**(2),133-144. https://doi.org/10.12989/cac.2020.25.2.133.

Aydogdu, M. (2008), "Conditions for functionally graded plates to remain flat under in-plane loads by classical plate theory", *Compos. Struct.*, **82**(1), 155-157.

https://doi.org/10.1016/j.compstruct.2006.10.004.
Bourada, F., Bousahla, A.A., Tounsi, A., Bedia, E.A.A., Mahmoud, S.R., Benrahou, K.H. and Tounsi, A. (2020), "Stability and dynamic analyses of SW-CNT reinforced concrete beam resting on elastic-foundation", *Comput. Concrete, Int. J.*, **25**(6), 485-495. https://doi.org/10.12989/cac.2020.25.6.485.
Bousahla, A.A., Bourada, F., Mahmoud, S.R., Tounsi, A., Algarni, A., Adda Bedia, E.A. and Tounsi, A. (2020), "Buckling and dynamic behavior of the simply supported CNT-RC beams using an integral-first shear deformation theory", *Comput. Concrete, Int. J.*, **25**(2), 155-166. https://doi.org/10.12989/cac.2020.25.2.155.
Chan, D.Q., Nguyen, P.D., Quang, V.D., Anh, V.T.T. and Duc, D.D. (2019), "Nonlinear buckling and post-buckling of functionally graded CNTs reinforced composite truncated conical shells subjected to axial load", *Steel Compos. Struct., Int. J.*, **31**(3), 243-259. https://doi.org/10.12989/scs.2019.31.3.243.
Draiche, K., Bousahla, A.A., Tounsi, A., Alwabli, A.S., Tounsi, A. and Mahmoud, S.R. (2019), "Static analysis of laminated reinforced composite plates using a simple first-order shear deformation theory", *Comput. Concrete, Int. J.*, **24**(4), 369-378. http://dx.doi.org/10.12989/cac.2019.24.4.369.
Draoui, A., Zidour M., Tounsi, A. and Adim, B. (2019), "Static and dynamic behavior of nanotubes-reinforced sandwich plates using FSDT", *J. Nano Res. S.W.*, **57**, 117-135. https://doi.org/10.4028/www.scientific.net/JNanoR.57.117.
Ebrahimi, F. and Farazmandnia, N. (2018a), "Vibration analysis of functionally graded carbon nanotube-reinforced composite sandwich beams in thermal environment", *Adv. Aircr. Spacecr. Sci., Int. J.*, **5**(1), 107-128. https://doi.org/10.12989/aas.2018.5.1.107.
Ebrahimi, F. and Farazmandnia, N. (2018b), "Thermal buckling analysis of functionally graded carbon nanotube-reinforced composite sandwich beams", *Steel Compos. Struct., Int. J.*, **27**(2), 149-159. https://doi.org/10.12989/scs.2018.27.2.149.
Ebrahimi, F., Nouraei, M., Dabbagh, A. and Timon Rabczuk, T. (2019), "Thermal buckling analysis of embedded graphene-oxide powder-reinforced nanocomposite plates", *Adv. Nano Res., Int. J.*, **7**(5), 293-310. https://doi.org/10.12989/anr.2019.7.5.293.
Garcia, E.M., Rodriguez, L.T., Castro, R.T. and Andres, S. (2017), "Buckling analysis of functionally graded carbon nanotube reinforced curved panels under axial compression and shear", *Compos. Part B*, **108**(1), 243-256. https://doi.org/10.1016/j.compositesb.2016.10.002.
Han, Y. and Elliott, J. (2007), "Molecular dynamics simulations of the elastic properties of polymer/carbon nanotube composites", *Comput. Mater. Sci.*, **39**(2), 315-323. https://doi.org/10.1016/j.commatsci.2006.06.011.
Hieu, P.T. and Tung, H.V. (2018), "Post-buckling behavior of CNT-reinforced composite cylindrical shell surrounded by an elastic medium and subjected to combined mechanical loads in thermal environments", *J. Therm. Compos. Mater.*, **32**(10), 1319-1346. https://doi.org/10.1177/0892705718796551.
Hieu, P.T. and Tung, H.V. (2020), "Thermal and thermomechanical buckling of shear deformable FG-CNTRC cylindrical shells and toroidal shell segments with tangentially restrained edges", *J. Arch. Appl. Mech.*, **90**, 1529-1546. https://doi.org/10.1007/s00419-020-01682-7.
Hussain, M., Naeem, M.N., Tounsi, A. and Taj, M. (2019), "Nonlocal effect on the vibration of armchair and zigzag SWCNTs with bending rigidity", *Adv. Nano Res., Int. J.*, **7**(6), 431-442. https://doi.org/10.12989/anr.2019.7.6.431.
Hussain, M., Naeem, M.N., Taj, M. and Tounsi, A. (2020), "Simulating vibration of single-walled carbon nanotube using Rayleigh-Ritz's method", *Adv. Nano Res., Int. J.*, **8**(3), 215-228. https://doi.org/10.12989/anr.2020.8.3.215.
Jones, R.M. (2005), "Thermal buckling of uniformly heated unidirectional and symmetric cross-ply laminated fiber-reinforced composite uniaxial in-plane restrained simply supported rectangular plates", *Compos. A Appl. Sci. Manuf.*, **36**(10), 1355-1367. https://doi.org/10.1016/j.compositesa.2005.01.028.
Kaddari, M., Kaci, A., Bousahla, A.A., Tounsi, A., Bourada, F., Tounsi, A. and Al-Osta, M.A. (2020), "A study on the structural behaviour of functionally graded porous plates on elastic foundation using a new quasi-3D model: Bending and free vibration analysis", *Comput. Concrete, Int. J.*, **25**(1), 37-57. https://doi.org/10.12989/cac.2020.25.1.037
Karami, B. and Karami, S. (2019), "Buckling analysis of nanoplate-type temperature-dependent heterogeneous materials", *Adv. Nano Res., Int. J.*, **7**(1), 51-61. https://doi.org/10.12989/anr.2019.7.1.051.
Khiloun, M., Bousahla, A.A., Kaci, A., Bessaim, A., Tounsi, A. and Mahmoud, S.R. (2020), "Analytical modeling of bending and vibration of thick advanced composite plates using a four-variable quasi 3D HSDT", *Eng. Comput.*, **36**, 807-821. https://doi.org/10.1007/s00366-019-00732-1.
Kiani, Y. (2016), "Thermal post-buckling of temperature-dependent sandwich beams with carbon nanotube-reinforced face sheets", *J. Therm. Stresses*, **39**(9), 1098-1110. https://doi.org/10.1080/01495739.2016.1192856.
Kiani, Y. (2017a), "Thermal buckling of temperature-dependent FG-CNT-reinforced composite skew plates", *J. Therm. Stresses*, **40**(11), 1442-1460. https://doi.org/10.1080/01495739.2017.1336742.
Kiani, Y. (2017b), "Thermal post-buckling of FG-CNT reinforced composite plates", *Compos. Struct.*, **159**(1), 299-306. https://doi.org/10.1016/j.compstruct.2016.09.084.
Kiani, Y. (2018), "Thermal post-buckling of temperature dependent sandwich plates with FG-CNTRC face sheets", *J. Therm. Stresses*, **41**(7), 866-882. https://doi.org/10.1080/01495739.2018.1425645.
Kiani, Y., Dimitri, R. and Tornabene, F. (2018), "Free vibration study of composite conical panels reinforced with FG-CNTs", *Eng. Struct.*, **172**, 472-482. https://doi.org/10.1016/j.engstruct.2018.06.006.
Leissa, W. (1986), "Conditions for laminated plates to remain flat under inplane loading", *Compos. Struct.*, **6**(4), 261-270. https://doi.org/10.1016/0263-8223(86)90022-X.
Matouk, H., Bousahla, A.A., Heireche, H., Bourada, F., Bedia, E.A.A., Tounsi, A. and Benrahou, K.H. (2020), "Investigation on hygro-thermal vibration of P-FG and symmetric S-FG nanobeam using integral Timoshenko beam theory", *Adv. Nano Res., Int. J.*, **8**(4), 293-305. https://doi.org/10.12989/anr.2020.8.4.293.
Medani, M., Benahmed, A., Zidour, M., Heireche, H., Tounsi, A., Bousahla, A.A. and Mahmoud, S.R. (2019), "Static and dynamic behavior of (FG-CNT) reinforced porous sandwich plate using energy principle", *Steel Compos. Struct., Int. J.*, **32**(5), 595-610. https://doi.org/10.12989/scs.2019.32.5.595.
Mehar, M. and Panda, S.K. (2019), "Multiscale modeling approach for thermal buckling analysis of nanocomposite curved structure", *Adv. Nano Res., Int. J.*, **7**(3), 179-188. https://doi.org/10.12989/anr.2019.7.3.179.
Mirzaei, M. (2018), "Thermal buckling of temperature-dependent composite super elliptical plates reinforced with carbon nanotubes", *J. Therm. Stresses*, **41**(7), 920-935. https://doi.org/10.1080/01495739.2018.1429969.
Mirzaei, M. (2020), "Vibration of FG-CNT reinforced composite cylindrical panels with cutout", *Mech. Based Des. Struct. Mach.*, **41**(7), 920-935. https://doi.org/10.1080/15397734.2019.1705165.

Mirzaei, M. and Kiani, Y. (2016a), "Free vibration of functionally graded carbon nanotube reinforced composite cylindrical panels", *Compos. Struct.*, **142**(8), 45-56. https://doi.org/10.1016/j.compstruct.2015.12.071.

Mirzaei, M. and Kiani, Y. (2016b), "Thermal buckling of temperature dependent FG-CNT reinforced composite plates", *Meccanica*, **51**(9), 2185-2201. https://doi.org/10.1007/s11012-015-0348-0.

Qatu, M.S. and Leissa A.W. (1993), "Buckling or transverse deflections of unsymmetrically laminated plates subjected to in-plane loads", *AIAA J.*, **31**(1), https://doi.org/10.2514/3.11336.

Qin, B., Zhong, R., Wang, T., Wang, Q., Xu, Y. and Hu, Z. (2020), "A unified Fourier series solution for vibration analysis of FG-CNTRC cylindrical, conical shells and annular plates with arbitrary boundary conditions", *Compos. Struct.*, **232**(2), 111549. https://doi.org/10.1016/j.compstruct.2019.111549.

Reddy, J.N. (2003), *Mechanics of Laminated Composite Plates and Shells*, CRC Press, USA.

Rezaiee-Pajand, M., Mokhtari, M. and Hozhabrossadati, S.M. (2019), "Application of Hencky bar-chain model to buckling analysis of elastically restrained Timoshenko axially functionally graded carbon nanotube reinforced composite beams", *Mech. Based Des. Struct. Mach.*, **47**(5), 599-620. https://doi.org/10.1080/15397734.2019.1596129.

Shahedi, S. and Mohammadimehr, M. (2019), "Vibration analysis of rotating fully-bonded and delaminated sandwich beam with CNTRC face sheets and AL-foam flexible core in thermal and moisture environments", *Mech. Based Des. Struct. Mach.*, **48**(5), 584-614. https://doi.org/10.1080/15397734.2019.1646661.

Shen, H.S. (2009), "Nonlinear bending of functionally graded carbon nanotube reinforced composite plates in thermal environments", *Compos. Struct.*, **91**(1), 9-19. https://doi.org/10.1016/j.compstruct.2009.04.026.

Shen, H.S. (2016), "Post-buckling of nanotube-reinforced composite cylindrical panels resting on elastic foundations subjected to lateral pressure in thermal environments", *Eng. Struct.*, **122**(17), 174-183. https://doi.org/10.1016/j.engstruct.2016.05.004.

Shen, H.S. and Zhang, C.L. (2010), "Thermal buckling and post-buckling behavior of functionally graded carbon nanotube-reinforced composite plates", *Mater. Des.*, **31**(7), 3403-3411. https://doi.org/10.1016/j.matdes.2010.01.048.

Shen, H.S. and Xiang, Y. (2013), "Nonlinear analysis of nanotube reinforced composite beams resting on elastic foundations in thermal environments", *Eng. Struct.*, **56**(14), 698-708. https://doi.org/10.1016/j.engstruct.2013.06.002.

Shen, H.S. and He, X.Q. (2017), "Large amplitude free vibration of nanotube-reinforced composite doubly curved panels resting on elastic foundations in thermal environments", *J. Vib. Control*, **23**(16), 2672-2689. https://doi.org/10.1177/1077546315619280.

Shen, H.S. and Wang, H. (2017), "Nonlinear vibration of compressed and thermally post-buckled nanotube reinforced composite plates resting on elastic foundations", *Aerosp. Sci. Technol.*, **64**, 63-74. https://doi.org/10.1016/j.ast.2017.01.017.

Tayeb Si, T., Zidour, M., Bensattalah, T., Heireche, H., Benahmed, A. and Adda Bedia, E.A. (2020), "Mechanical buckling of FG-CNTs reinforced composite plate with parabolic distribution using Hamilton's energy principle", *Adv. Nano Res., Int. J.*, **8**(2), 135-148. https://doi.org/10.12989/anr.2020.8.2.135.

Torabi, J. and Ansari, R. (2018), "Thermally induced mechanical analysis of temperature-dependent FG-CNTRC conical shells", *Struct. Eng. Mech., Int. J.*, **68**(3), 313-323. https://doi.org/10.12989/sem.2018.68.3.313.

Torabi, J. and Ansari, R. (2020), "Numerical investigation on the buckling and vibration of cracked FG cylindrical panels based on the phase-field formulation", *Eng. Fract. Mech.*, **228**, 106895. https://doi.org/10.1016/j.engfracmech.2020.106895.

Trang, T.N. and Tung, H.V. (2018), "Nonlinear stability of CNT-reinforced composite cylindrical panels with elastically restrained straight edges under combined thermomechanical loading conditions", *J. Therm. Compos. Mater.*, **33**(2), 153-179. https://doi.org/10.1177/0892705718805134.

Tung, H.V. and Trang, T.N. (2018), "Thermal post-buckling of shear deformable CNT reinforced composite plates with tangentially restrained edges and temperature dependent properties", *J. Therm. Compos. Mater.*, **33**(1), 97-124. https://doi.org/10.1177/0892705718804588.

Yazdi, A.A. (2019), "Nonlinear aeroelastic stability analysis of three-phase nano-composite plates", *Mech. Based Des. Struct. Mach.*, **47**(6), 753-768. https://doi.org/10.1080/15397734.2019.1610436.

Zarga, D., Tounsi, A., Bousahla, A.A., Bourada, F. and Mahmoud, S.R. (2019), "Thermomechanical bending study for functionally graded sandwich plates using a simple quasi-3D shear deformation theory", *Steel Compos. Struct., Int. J.*, **32**(3), 389-410. https://doi.org/10.12989/scs.2019.32.3.389.

Zhang, L.W. and Liew, K.M. (2016), "Post-buckling analysis of axially compressed CNT reinforced functionally graded composite plates resting on Pasternak foundations using an element-free approach", *Compos. Struct.*, **138**(4), 40-51. https://doi.org/10.1016/j.compstruct.2015.11.031.

Zhang, L.W. and Xiao, L.N. (2017), "Mechanical behavior of laminated CNT-reinforced composite skew plates subjected to dynamic loading", *Compos. Part B Eng.*, **122**, 219-30. https://doi.org/10.1016/j.compositesb.2017.03.041.

Zhang, L.W., Liew, K.M. and Reddy, J.N. (2016), "Post-buckling of carbon nanotube reinforced functionally graded plates with edges elastically restrained against translation and rotation under axial compression", *Comput. Methods Appl. Mech. Eng.*, **298**(1), 1-28. https://doi.org/10.1016/j.cma.2015.09.016.

AT